Supplementary Information for

Ab initio thermodynamics of liquid and solid water

Bingqing Cheng, Edgar A. Engel, Jörg Behler, Christoph Dellago, and Michele Ceriotti

Corresponding Author Name.
E-mail: bingqing.cheng@epfl.ch

This PDF file includes:

    Supplementary text
    Figs. S1 to S4
    Captions for Databases S1 to S3
    References for SI reference citations

Other supplementary materials for this manuscript include the following:

    Databases S1 to S3

187
188
189
190
191
192
193
194
195
196
197
198
199
200
201
202
203
204
205
206
207
208
209
210
211
212
213
214
215
216
217
218
219
220
221
222
223
224
225
226
227
228
229
230
231
232
233
234
235
236
237
238
239
240
241
242
243
244
245
246
247
248

125 **Supporting Information Text**

126
127 **1. The revPBE0-D3 DFT functional**

128 **A. Details of the DFT calculations.** Both the DFT calculations for constructing the data set used to train and benchmark the
129 NN potential, and for performing the free energy perturbation from NN to DFT, are performed using the CP2K code (1). We
130 use the revPBE0 (2–4) functional, which incorporates 25% of exact exchange, and a Grimme D3 dispersion correction (5, 6).
131 Computational details of the calculations are the same as those used in Ref. (7). We have also attached the CP2K input file as
132 a part of the supplemental information.

133
134 **B. The difference in lattice energy between ordered ice Ih and ice Ic.** We compute lattice energy of 1) the most stable proton
135 ordered form of Ih (XIh with space-group symmetry $Cmc2_1$), and 2) proton ordered cubic ice (Ic with space-group symmetry
136 $I4_1md$). Since CP2K currently only supports Γ-point calculations for hybrid functionals, these calculations are performed for
137 64-molecule $2 \times 2 \times 2$ supercells of the conventional 8-molecule orthorhombic unit cells. We perform geometrical optimization
138 at a few different volumes close to the equilibrium volume of each system, with the optimized cell shape. We find that an
139 equivalent plane-wave energy cutoff of $1200Ry$ ensures a smooth energy-volume curve, although the difference in the lattice
140 energy $U^{I4_1md} - U^{Cmc2_1} = -0.3\,\text{meV/H}_2\text{O}$ is already converged at $800Ry$.

141
142 **2. Construction of the neural network potential**

143 **A. Architecture of the NN potential.** The high-dimensional neural network potential for water, which is flexible and fully
144 dissociable, has been constructed using the method proposed by Behler and Parrinello (8). In this approach the total energy of
145 the system is determined as a sum of environment-dependent atomic energies. For each atom in the system, the positions of
146 all neighboring atoms inside a cutoff radius, which has to be converged, are described by a set of atom-centered many-body
147 symmetry functions (9). These sets of function values are then used as input vectors for the atomic neural networks yielding
148 the atomic energy contributions. Consequently, the analytic total energy expression is a sum over the outputs of all individual
149 atomic neural networks, and analytic gradients for the calculation of the forces are readily available.

150 Atomic environments within a cutoff radius of 12.0 a.u. are described using the symmetry function sets for hydrogen (27
151 functions) and oxygen (30 functions) atoms, selected by Morawietz et al. (10) in previous work on neural network potentials for
152 water employing GGA-DFT reference data. The hydrogen and oxygen atomic NNs consist of two hidden layers with 20 nodes
153 each. We have used the total energies and all force components present in the training set.

154
155 **B. The training set of the NN potential.** The construction and the selection of the training set is of crucial importance in making
156 an accurate and stable NN potential. In essence, the NN potential stores the shape of the PES as a set of fitting parameters,
157 which have been adjusted to the reference training set. When employing the NN in an atomistic simulation, the accuracy of the
158 predicted energy and forces for a given atomic environment is dictated by the structural similarity between this environment
159 and the ones contained the the reference set. If the given atomic environment is distant from anything the NN has been trained
160 on, the prediction will have a large error bar. Inaccurate energy predictions, in particular, tend to lead the system to explore
161 an un-physical part of the phase space.

162 In our reference set of the neural network, there are a total of 1,593 64-molecule bulk liquid water structures. During the
163 NN training, these were randomly split into a training set of 80% of the structures to determine the NN parameters, and a test
164 set of the rest 20% structures to estimate the quality of the NN potential and to help avoid over-fitting. We have released the
165 whole reference set on the (to be inserted) public repository.

166 The first 1,000 structures in the training set were selected in order to cover a large part of the configurational space of
167 possible atomic environment, which is reflected in the relatively large spread in their energies. The remaining 593 structures
168 were extracted from PIMD simulations at about 300 K.

169 At the end of the NN fitting procedure, a root-mean-square errors of $\approx 7\,\text{meV/H}_2\text{O}$ in energies and $\approx 120\,\text{meV/Å}$ in
170 forces are obtained for the test set. These errors are larger compared to those quoted for previous NN fits of water (about
171 $\approx 3\,\text{meV/H}_2\text{O}$ in energies and $\approx 110\,\text{meV/Å}$ in forces (11)). However, this is simply due to the larger structural (and energetic)
172 diversity of our test (and training) set. When comparing the predictions of the NN potential and revPBE0-D3 calculations for
173 configurations generated from MD and PIMD simulations for liquid water at 300 K, the root-mean-square errors of energies
174 and forces are $\approx 2\,\text{meV/H}_2\text{O}$ and $\approx 110\,\text{meV/Å}$, respectively.

175 The NN potentials generated from our training set are not only very accurate, but also highly stable: MD simulations of
176 bulk water can be performed at high temperatures of 800 K.

177
178 **C. A comparison between CP2K and VASP for the training set.** In order to assess the intrinsic uncertainties in the revPBE0-D3
179 reference data arising from the computational details, the revPBE0-D3 energies of the first 1,000 structures in the training set
180 were re-computed with VASP (12), using the hard PAW potentials at the Γ-point with a plane wave cutoff of 700 eV. Apart
181 from an obvious outlier which may result from an under-convergence of the self-consistent cycle, the agreement between the
182 results from CP2K and from VASP is very good. After removing the outlier, we measured the root-mean-square error of
183 energies between the results from the two codes to be $6\,\text{meV/H}_2\text{O}$ for the first 1000 configurations of the training set, which is
184 smaller compared with the training error of the NN potential.

185 Considering the subtle difference in predictions from different DFT codes and pseudopotentials (13), we are encouraged by
186 the agreement between CP2K and VASP for the hybrid revPBE0-D3 functional.

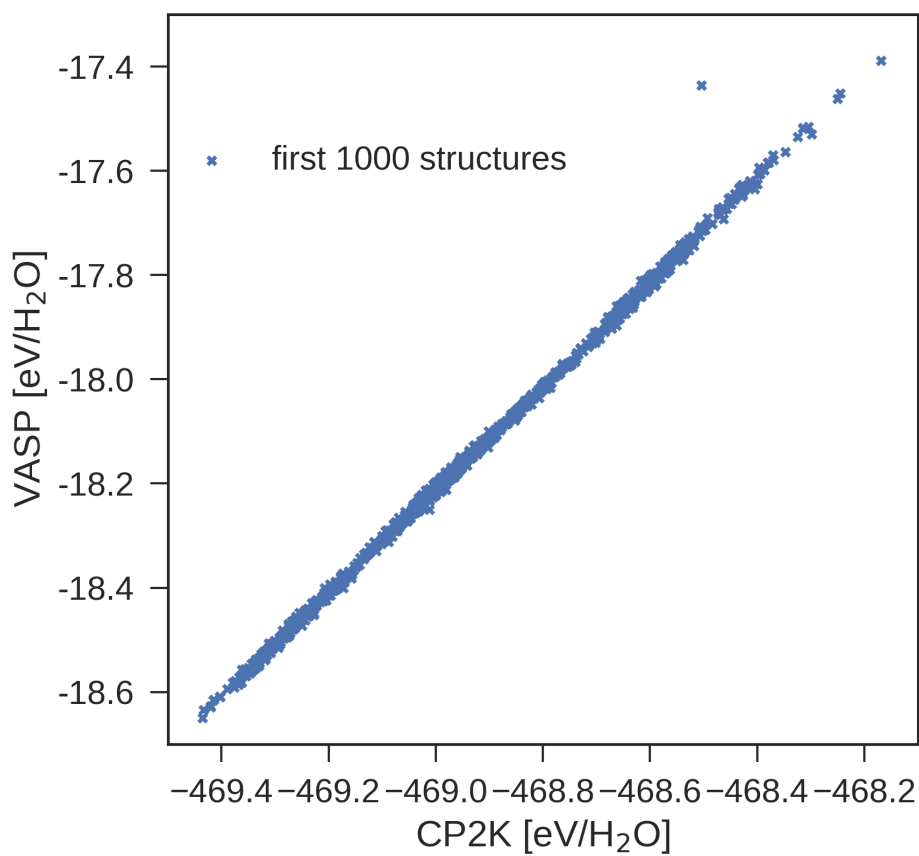**Bingqing Cheng, Edgar A. Engel, Jörg Behler, Christoph Dellago, and Michele Ceriotti**

Fig. S1. A comparison between the revPBE0-D3 energies computed using CP2K and using VASP.

D. A comparison between CP2K and MB-Pol for the training set. We have also compared our revPBE0-D3 energies to those obtained from the well-established MB-pol water potential (14), which has been demonstrated to accurately reproduce the structural, dynamical and thermodynamical properties of liquid water and many phases of ice (14). Because the MB-pol water is non-dissociative and not designed for highly displaced hydrogen atoms (e.g. in water undergoing autoprotolysis), but the first 1000 structures in the training set include such configurations, we have re-computed the energies for the last 593 structures in the training set, which was extracted from PIMD simulations. The agreement for these structures is excellent (the root-mean-square error of energies is $2.6\,\mathrm{meV/H_2O}$).

For completeness, we have further computed the MB-pol lattice energies of the proton-ordered forms of Ih and Ic with $Cmc2_1$ and $I4_1md$ symmetry, respectively, for which diffusion Monte Carlo (DMC) (15) and random phase approximation (RPA) (16) values are available for reference. Geometry-optimizations performed for the MB-pol optimized simulation cells (with molar volumes of $31.2\,\text{Å}^3$ and $31.6\,\text{Å}^3$ for Ih $Cmc2_1$ and Ic $I41_md$, respectively) suggest that Ih $Cmc2_1$ is $2\,\mathrm{meV/H_2O}$ more stable than Ic $I41_md$. It is worth noting that upon geometry optimization the $Cmc2_1$ of the initial Ih structure is broken. This is in disagreement both with experiment (that finds the most stable proton-ordered form of Ih (XIh) to possess $Cmc2_1$ symmetry (17)) and the results of DFT studies employing diverse density functionals, including revPBE0-D3. Meanwhile Ic $I4_1md$ retains its symmetry in geometry optimizations.

E. The enthalpy of water based on the NN potential. In Figure S3 we plot the enthalpy of ice Ih, Ic and liquid water systems computed from NPT simulations at 1 bar.

3. Comparison between two neural network potentials

Bingqing Cheng, Edgar A. Engel, Jörg Behler, Christoph Dellago, and Michele Ceriotti

497
498
499
500
501
502
503
504
505
506
507
508
509
510
511
512
513
514
515
516
517
518
519
520
521
522
523
524
525
526
527
528
529
530
531
532
533
534
535
536
537
538
539
540
541
542
543
544
545
546
547
548
549
550
551
552
553
554
555
556
557
558

559
560
561
562
563
564
565
566
567
568
569
570
571
572
573
574
575
576
577
578
579
580
581
582
583
584
585
586
587
588
589
590
591
592
593
594
595
596
597
598
599
600
601
602
603
604
605
606
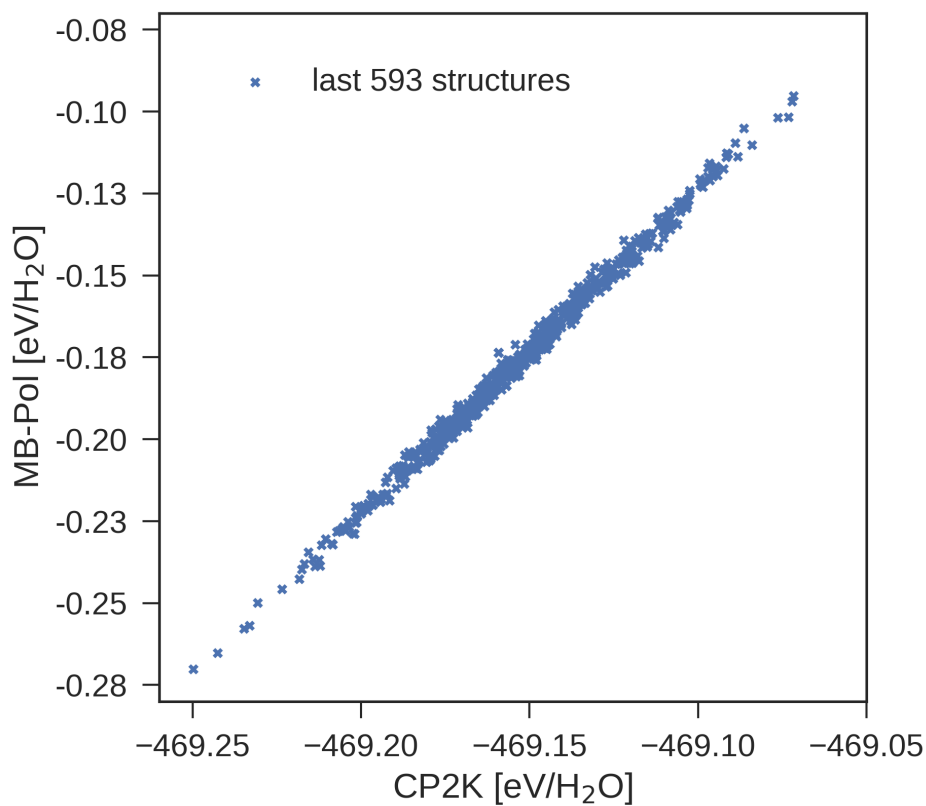607
608
609
610
611
612
613
614
615
616
617
618
619
620

Fig. S2. A comparison between the revPBE0-D3 energies computed using CP2K, and the energies computed using the MB-Pol potential.

621
622
623
624
625
626
627
628
629
630
631
632
633
634
635
636
637
638
639
640
641
642
643
644
645
646
647
648
649
650
651
652
653
654
655
656
657
658
659
660
661
662
663
664
665
666
667
668
669
670
671
672
673
674
675
676
677
678
679
680
681
682

683
684
685
686
687
688
689
690
691
692
693
694
695
696
697
698
699
700
701
702
703
704
705
706
707
708
709
710
711
712
713
714
715
716
717
718
719
720
721
722
723
724
725
726
727
728
729
730
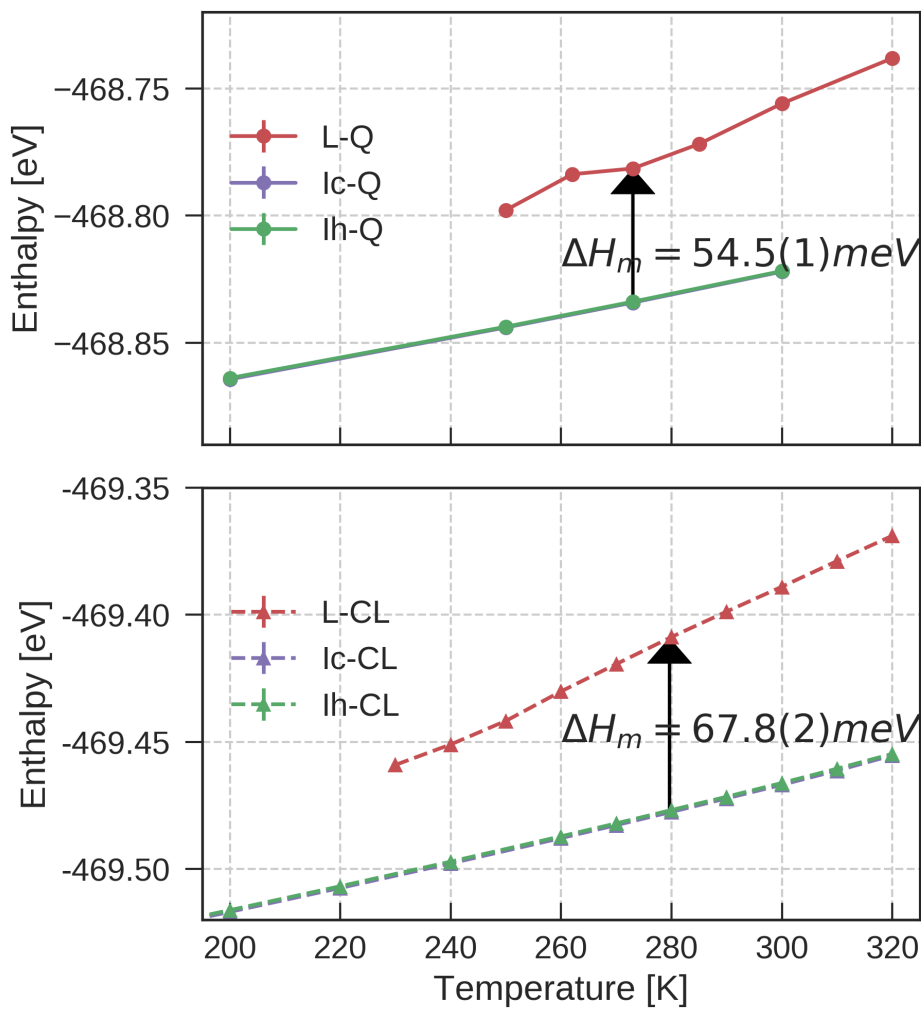731
732
733
734
735
736
737
738
739
740
741
742
743
744

Fig. S3. The enthalpy of the water systems described by the NN potential.

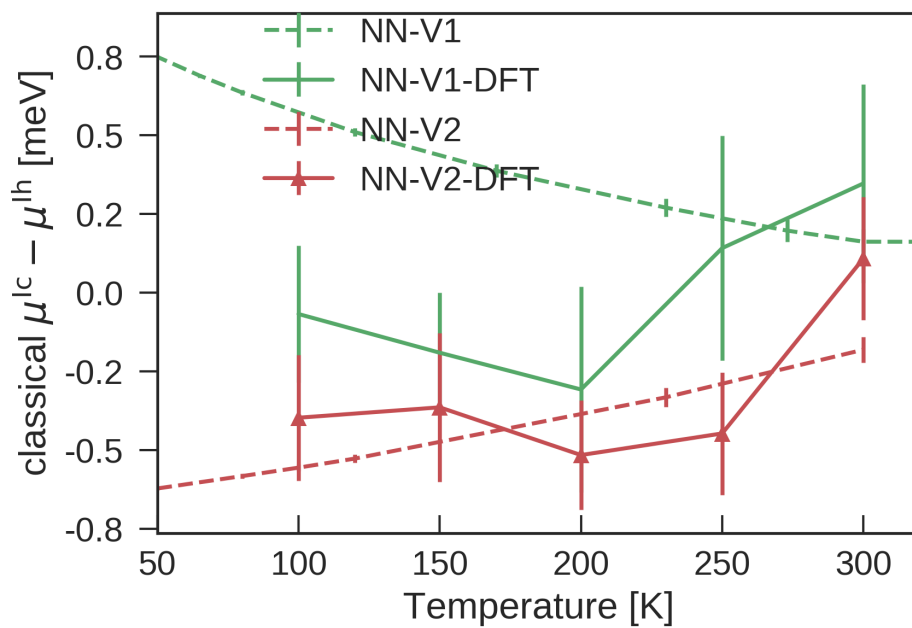**Bingqing Cheng, Edgar A. Engel, Jörg Behler, Christoph Dellago, and Michele Ceriotti**

Fig. S4. The chemical potential difference between ice Ih and Ic predicted using two different neural network potentials (NN-V1 and NN-V2).

We have trained several NN potentials for the same underlying revPBE0-D3 DFT reference using different training sets and/or initial random seeds. In general, we notice subtle differences in the predictions of different neural networks. This is due to that, as mentioned in the main text, the fitting strategy for the NN, the finite cut-off radii applied to the description of atomic environments, and possible "holes" in the training set (18) inevitably lead to small residual errors between NN predictions and those obtained at the first-principles level of theory on which the NN is based.

To quantify the differences between different NN potentials, we select two NN potentials: (i) the first version of the NN (NN-V1) was trained using the first 1,000 liquid structures in the reference set, and (2) a refined version (NN-V2) was trained using all the 1,593 reference structures. NN-V2 is the NN that is actually employed in the simulations described in the main text.

Using each of the NN potential, we compute the chemical potential difference $\Delta\mu_{\text{cl}}^{\text{Ih}\rightarrow\text{Ic}}$ between ice Ih and Ic at the classical level, following the steps and simulation setups described in the main text. It can be seen from Figure S4, the predictions on the chemical potential difference $\Delta\mu_{\text{cl,NN}}^{\text{Ih}\rightarrow\text{Ic}}$ from the two neural networks differ by as much as $1\,\text{meV}/\text{H}_2\text{O}$. However, after we promote the results back to the DFT level and obtain $\Delta\mu_{\text{cl}}^{\text{Ih}\rightarrow\text{Ic}}$, the discrepancy in the predictions largely diminished.

4. Predicting The chemical potential difference between ice Ih and Ic using the MB-Pol potential

We perform a thermodynamic integration in the NPT ensemble, using a parameter λ to perform the switching between the NN Hamiltonian $\mathcal{H}_{\text{NN}}$ and the MB-Pol (14) Hamiltonian $\mathcal{H}_{\text{MB}}$. In practice, we run multiple simulations with the Hamiltonian $\mathcal{H}(\lambda) = (1-\lambda)\mathcal{H}_{\text{NN}} + \lambda\mathcal{H}_{\text{MB}}$ at $\lambda = 0.0, 0.2, 0.8, 1.0$. The MB-Pol free energies of the ice Ic and Ih systems with 768 molecules described in the main text is evaluated using

$$G_{\text{MB}}(P,T) - G_{\text{NN}}(P,T) = \int_0^1 d\lambda \left\langle U_{\text{MB}} - U_{\text{NN}} \right\rangle_{P,T,\lambda}, \qquad [1]$$

where $\langle\ldots\rangle_{P,T,\lambda}$ denotes the ensemble average over NPT simulations using the Hamiltonian $H(\lambda)$. As the PESs described by MB-Pol and NN are extremely close, the integral in Eqn. Eq. (1) can be converged to below $0.01\,\text{meV}$ from simulations of less than 100 picoseconds in total. We find that the difference between the classical chemical potentials of ice Ic and Ih using the MB-Pol potential is $0.2\,\text{meV}/\text{H}_2\text{O}$ lower than the classical NN prediction $\Delta\mu_{\text{cl,NN}}^{\text{Ih}\rightarrow\text{Ic}}$.

5. Other supplementary files

We have uploaded the following data files to the Materials Cloud repository
https://archive.materialscloud.org/2018.0020/v1
and a GitHub repository
https://github.com/BingqingCheng/ab-initio-thermodynamics-of-water.
Additional data table S1 (NN-potential)
    Parameters for the water neural network potential based on revPBE0-D3 DFT. Instructions and examples for running MD using this potential

Additional data table S2 (training-set)
    The training (and test) set of the NN potential, including atomic configurations, energies, and forces. We have provided two formats: "input.data" is suitable for training NN potentials using the RuNNer code (19) or the N2P2 code (20, 21), and "dataset_1593.xyz" is in a libatom xyz format.

Additional data table S3 (input-files)
    We have uploaded the necessary input files for all the simulations (e.g. thermodynamic integration, path-integral molecular dynamics, interface pinning), as well as a Python notebook to help data analysis for the thermodynamic integration method.

References

1. Lippert G, Hutter J, Parrinello M (1999) The Gaussian and augmented-plane-wave density functional method for ab initio molecular dynamics simulations. *Theoretical Chemistry Accounts* 103:124.
2. Zhang Y, Yang W (1998) Comment on "Generalized Gradient Approximation Made Simple". *Physical Review Letters* 80:890.
3. Adamo C, Barone V (1999) Toward reliable density functional methods without adjustable parameters: The PBE0 model. *Journal of Chemical Physics* 110:6158.
4. Goerigk L, Grimme S (2011) A thorough benchmark of density functional methods for general main group thermochemistry, kinetics, and noncovalent interactions. *Physical Chemistry Chemical Physics* 13:6670.
5. Grimme S, Antony J, Ehrlich S, Krieg S (2010) A consistent and accurate ab initio parametrization of density functional dispersion correction (dft-d) for the 94 elements H-Pu. *Journal of Chemical Physics* 132:154104.
6. Goerigk L, Grimme S (2011) A thorough benchmark of density functional methods for general main group thermochemistry, kinetics, and noncovalent interactions. *Physical Chemistry Chemical Physics* 13(14):6670–6688.

Bingqing Cheng, Edgar A. Engel, Jörg Behler, Christoph Dellago, and Michele Ceriotti

7. Marsalek O, Markland TE (2017) Quantum Dynamics and Spectroscopy of Ab Initio Liquid Water: The Interplay of Nuclear and Electronic Quantum Effects. *J. Phys. Chem. Lett.* 8:1545.

8. Behler J, Parrinello M (2007) Generalized Neural-Network Representation of High-Dimensional Potential-Energy Surfaces. *Phys. Rev. Lett.* 98:146401.

9. Behler J (2011) Neural network potential-energy surfaces in chemistry: a tool for large-scale simulations. *PCCP* 13:17930–55.

10. Morawietz T, Singraber A, Dellago C, Behler J (2016) How van der waals interactions determine the unique properties of water. *Proceedings of the National Academy of Sciences* 113(30):8368–8373.

11. Imbalzano G, et al. (2018) Automatic selection of atomic fingerprints and reference configurations for machine-learning potentials. *The Journal of Chemical Physics* 148(24):241730.

12. Kresse G (1996) Software vasp, vienna, 1999; g. kresse, j. furthmüller. *Phys. Rev. B* 54(11):169.

13. Lejaeghere K, et al. (2016) Reproducibility in density functional theory calculations of solids. *Science* 351(6280):aad3000.

14. Reddy SK, et al. (2016) On the accuracy of the mb-pol many-body potential for water: Interaction energies, vibrational frequencies, and classical thermodynamic and dynamical properties from clusters to liquid water and ice. *The Journal of chemical physics* 145(19):194504.

15. Raza Z, et al. (2011) Proton ordering in cubic ice and hexagonal ice; a potential new ice phase – XIc. *Physical Chemistry Chemical Physics* 13:19788–19795.

16. Macher M, Klimeš J, Franchini C, Kresse G (2014) The random phase approximation applied to ice. *The Journal of Chemical Physics* 140(8):084502.

17. Jackson SM, Nield VM, Whitworth RW, Oguro M, Wilson CC (1997) Single-crystal neutron diffraction studies of the structure of ice XI. *Journal of Physical Chemistry B* 101:6142.

18. Behler J (2015) Constructing high-dimensional neural network potentials: A tutorial review. *International Journal of Quantum Chemistry* 115(16):1032–1050.

19. Behler J (2018) *RuNNer – A Neural Network Code for High-Dimensional Neural Network Potentials*. (Universität Göttingen).

20. Singraber A, Behler J, Dellago C (In press) A library-based lammps implementation of high-dimensional neural network potentials. *The Journal of Chemical Theory and Computation*.

21. Singraber A (2018) Compphysvienna/n2p2: Neural network potential package 1.0.0.